

The Doubling of Stellar Black Hole Nuclei

Mher V. Kazandjian^{1*} and J. R. Touma^{2*}

¹*Leiden Observatory, Leiden University, P.O. Box 9513, 2300 RA Leiden, The Netherlands*

²*Department of Physics, American University of Beirut, Beirut, Lebanon*

Accepted yyyy mmmmmmmm dd. Received yyyy mmmmmmmm dd; in original form yyyy mmmmmmmm xx

ABSTRACT

It is strongly believed that Andromeda’s double nucleus signals a disk of stars revolving around its central super-massive black hole on eccentric Keplerian orbits with nearly aligned apsides. A self-consistent stellar dynamical origin for such apparently long-lived alignment has so far been lacking, with indications that cluster self-gravity is capable of sustaining such lopsided configurations if and when stimulated by external perturbations. Here, we present results of N-body simulations which show unstable counter-rotating stellar clusters around super-massive black holes saturating into uniformly precessing lopsided nuclei. The double nucleus in our featured experiment decomposes naturally into a thick eccentric disk of apo-apse aligned stars which is embedded in a lighter triaxial cluster. The eccentric disk reproduces key features of Keplerian disk models of Andromeda’s double nucleus; the triaxial cluster has a distinctive kinematic signature which is evident in HST observations of Andromeda’s double nucleus, and has been difficult to reproduce with Keplerian disks alone. Our simulations demonstrate how the combination of eccentric disk and triaxial cluster arises naturally when a star cluster accreted over a pre-existing and counter-rotating disk of stars, drives disk and cluster into a mutually destabilizing dance. Such accretion events are inherent to standard galaxy formation scenarios. They are here shown to double stellar black hole nuclei as they feed them.

Key words: galaxies:nuclei – galaxies:kinematics and dynamics – instabilities.

1 INTRODUCTION

Over the years, the nucleus of the Andromeda galaxy (M31) went from being asymmetric, to doubling, then tripling. The asymmetry was first noted in the balloon-born Stratoscope observatory (Light et al. 1974). It was photometrically resolved into a double nucleus by Hubble Space Telescope (HST) observations (Lauer et al. 1993); asymmetry hence turned into lopsidedness, with a luminous feature (referred to as P1) shining a few parsecs away from a dimmer one (referred to as P2), which is closer to the center of the host bulge. The resolved double nucleus had already been suspected to host a Super-Massive Black Hole (SMBH), located somewhere close to P2, with a neighborhood that was known to shine brighter than the rest of the nucleus in the ultraviolet (Dressler & Richstone 1988; Kormendy 1988). Detailed HST spectroscopy added a third component (known as P3), a disk of young massive stars, whose size and rotation speed rules out viable alternatives to a central SMBH of $\sim 10^8$ solar masses (M_{\odot}) (Bender et al. 2005).

In the currently favored model of M31’s lopsided double nucleus (Tremaine 1995; Peiris & Tremaine 2003), the

brighter peak P1 (Lauer et al. 1993) is thought to coincide with the common apo-centric region of an eccentric disc of stars revolving on nearly apse-aligned Keplerian ellipses, around M31’s central super-massive black hole (hereafter SMBH). Similar eccentric discs are thought to underlie lopsided nuclei detected around SMBHs in the centers of nearby galaxies (Lauer et al. 1996, 2005; Gültekin et al. 2011). That such kinematic configurations can be sustained in self-gravitating disks around SMBHs was clarified in a series of dynamical studies. Indeed, investigation of modes of hot nearly-Keplerian disks indicated that slow ($m=1$, lopsided) modes can be stably excited (Tremaine 2001). This conclusion was corroborated by results of planar N-body simulations of disks around SMBHs which showed that, when started in asymmetric conditions, disks can relax into long-lived uniformly precessing lopsided configurations (Bacon et al. 2001; Jacobs & Sellwood 2001). Subsequently, razor-thin, self-gravitating, lopsided equilibria were constructed, yielding encouraging agreement with photometric and kinematic observations of M31’s nucleus (Salow & Statler 2001; Sambhus & Sridhar 2002). These and related studies left open questions about how such modes are excited, how they ultimately saturate into global lopsided configurations, and whether constructed equilibria

* E-mail: mher@strw.leidenuniv.nl; jt00@aub.edu.lb

were stable or not. The early suggestion (Tremaine 1995) that an initially circular disk could become eccentric under the influence of dynamical friction with the host bulge has not been thoroughly explored. A recently proposed scenario (Hopkins & Quataert 2010a,b) has eccentric disks forming in the notoriously complex -and poorly understood (Silk 2011)- environment which couples star formation and its feedback to gas accretion in the early stages of SMBH growth.

In this work, we opt for a minimalist and dynamically self-consistent route to three-dimensional, lopsided nuclei, out of counter-rotating (CR hereafter) collisionless stellar distributions dominated by SMBHs. Such CR distributions are prone to violent $m=1$ instabilities in the presence of moderate counter-rotation (Jog & Combes 2009; Touma 2002), hence the suggestion that the lopsided structure in Andromeda’s nucleus may have been triggered by the accretion of a retrograde globular cluster in a pre-existing disk of stars (Sambhus & Sridhar 2002). With the intention of exploring the outcomes of such accretion events, we performed a series of N-body simulations of CR stellar distributions evolving in the sphere of influence of an SMBH. Below, we report on results which show unstable CR distributions evolving into stable, uniformly precessing lopsided nuclei. We follow the instability in our featured simulation from multiple complementary perspectives. We then probe the ensuing lopsided nucleus, and show that in addition to displaying all the key observational signatures which Keplerian disks are meant to model, it recovers asymmetries in the tail of Adromeda’s line of sight velocity distribution (Bender et al. 2005) which a thick lopsided disk alone is unable to reproduce (Peiris & Tremaine 2003).

2 COUNTER-ROTATING INSTABILITY: FROM LINEAR GROWTH TO SATURATION

Our N-body simulations were performed with the parallel version of *Gadget-2* (Springel 2005), an oct-tree code, which is popular with the cosmological structure formation community. We pushed this tool to the limit of extreme mass ratios, one for which it was not specifically designed, one in which it did the desired job, albeit with stringent force accuracy, and time stepping criteria. With M31 in mind, all experiments have an SMBH with a mass of $M_{\bullet}=10^8 M_{\odot}$ and a main disk component (prograde in our convention) with a tenth of SMBH mass (Bender et al. 2005; Peiris & Tremaine 2003). An exhaustive exploration, with sufficient realism, of a scenario in which a CR cluster ($10^5 - 10^6 M_{\odot}$) decays under dynamical friction to nuclear regions (Tremaine et al. 1975), then gets disrupted (Kim & Morris 2003; Fujii et al. 2010) as it couples to the massive nuclear stellar disk, would have been forbidding to pursue in detail with our current computational resources. Instead we opted for an extensive exploration of a realistic configuration which is known to be unstable (Touma 2002; Sridhar & Saini 2010), and in which the disrupted CR cluster is modeled by overlaying the prograde disk with a retrograde disk of 1/10 its mass. Details on initial conditions for this experiment, along with *Gadget-2* simulation parameters, are described in Appendix A; vari-

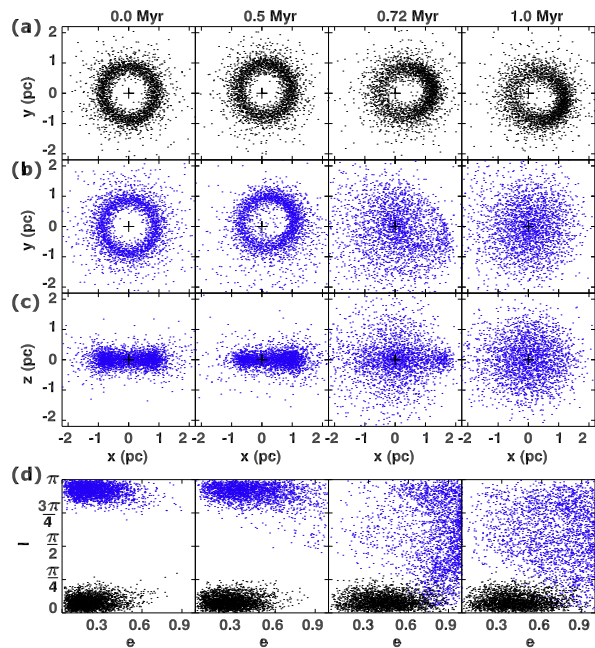


Figure 1. The eccentricity-inclination dynamics of the particles up to 1 Myr is shown. In row **a**, we follow a top view of the prograde particles, from initial axisymmetric annular configuration, through a phase of growth of lopsidedness, with growing mean eccentricity (0.41 around 1 Myrs), and alignment of apses. Row **b** shows a top view of retrograde particles over the same period; they experience greater increase in mean eccentricity (around 0.73 by 0.72 Myrs), and show signs of apse alignment by 0.5 Myrs, before dispersing (by 1 Myrs) into a disky blob. A side view of retrograde particles in row **c** shows how the in-plane dispersal seen in row **b** reflects in projection a burst of out-of-plane dynamics which puffs the initially retrograde disk into a triaxial cluster of stars. The eccentricity-inclination dynamics of the full cluster is captured in row **d**, with prograde in black, and retrograde in blue; the mean eccentricity of both populations grows as the instability develops; by 1 Myrs, the mean inclination of the prograde particles has hardly changed, while the highly eccentric retrograde population, is widely dispersed in inclination.

ations on the fiducial experiment are discussed in Appendix B.

2.1 Dissecting the Instability

CR configurations are known to be (linearly) unstable (Touma 2002; Sridhar & Saini 2010). We are here concerned with the (non-linear) saturation of this instability and shall first map its unfolding with complementary views of particle dynamics (Fig. 1). A top view of stars, in both prograde and retrograde populations (hereafter PP and RP respectively), shows them developing lopsidedness by coupling growing eccentricity to apse-alignment. The more massive PP maintains its coherent, apse-aligned precession (Fig. 1,(a)) whereas the lighter RP dissolves gradually into a disky blob after 0.5 Myrs (Fig. 1,(b)). Viewed from the side, the gradual in-plane dispersal of the RP occurs along with a dramatic excitation of out-of-plane motion; by 1 Myrs the RP unfolds into a triaxial structure (Fig. 1,(c)). Scatter plots of particle eccentricities and inclinations (Fig. 1,(d))

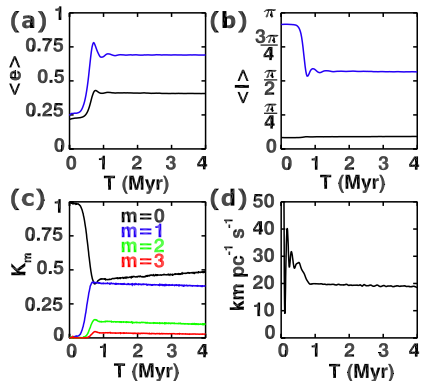


Figure 2. The linearly unstable, counter-rotating configuration saturates into a lopsided uniformly precessing disk. Panels **a** and **b** show the mean eccentricity $\langle e \rangle$ and inclination $\langle I \rangle$ of PP (black) and RP (blue). $\langle e \rangle$ grows, at near constant $\langle I \rangle$, till about 0.5 Myrs, at which point $\langle I \rangle$ takes off, with both $\langle e \rangle$ and $\langle I \rangle$ peaking around 0.72 Myrs. Cycles of increasingly smaller amplitude follow this initial growth phase, leading to a saturated eccentric prograde disk which is shrouded by a triaxial halo. In panel **c**, the power of the four dominant modes in projected density is displayed; an initially axisymmetric configuration ($m=0$) lends way to a dominant $m=1$ mode, along with non-negligible $m=2$ and $m=3$ contributions. Triaxial dispersal of the RP is responsible for the slight growth of the $m=0$ amplitude, and the related slight decrease in the $m=1$ mode amplitude after 0.72 Myrs. In panel **d**, we follow the precession rate of the $m=1$ mode in time: initial large amplitude oscillations reflect back and forth libration of prograde and retrograde $m=1$ excitations about the uniform precession state; these oscillations die out with the dispersal of the retrograde bunch, leaving an $m=1$ mode which precesses at a near constant rate of $19 \text{ km s}^{-1} \text{ pc}^{-1}$.

reveal how, by 0.72 Myrs, the now highly eccentric RP is well on its way to complete triaxial disruption. Tucked in this emerging cluster, the PP, which has absorbed much of the RP’s (negative) angular momentum, heats up slightly in inclination as it consolidates its eccentric lump, then adjusts slowly to whatever little angular momentum is left in the RP.

A look at the mean eccentricity and inclination of both populations (Fig. 2 **a**, **b**) confirms these observations, as it reveals three distinct phases: **Phase-I** of near coplanar growth of the mean eccentricity of both populations which lasts till about 0.5 Myrs; **Phase-II** of continued mean eccentricity growth, but now coupled to growth in the mean inclination of the RP, both of which reach a maximum around 0.72 Myr; **Phase-III**, with cycles of increasingly small amplitude leading to a near-steady regime. As emphasized in the caption of Fig. 2, transitions in mean eccentricity and inclination are neatly imprinted on the modal structure of the projected density and the pattern speed of the dominant $m=1$ mode, as the full cluster transitions from a thin axisymmetric initial state, to a saturated, lopsided, and slowly precessing mode (Fig. 2, **c**, **d**, and Fig. 3).

Saturation of the $m=1$ mode is evidently correlated with the dispersal of the initially retrograde population into a triaxial cluster of high eccentricity orbits. The dispersal appears to be associated with collective dynamics along eccentricity-inclination cycles. These cycles are excited when a population of stars (the retrograde population) develops

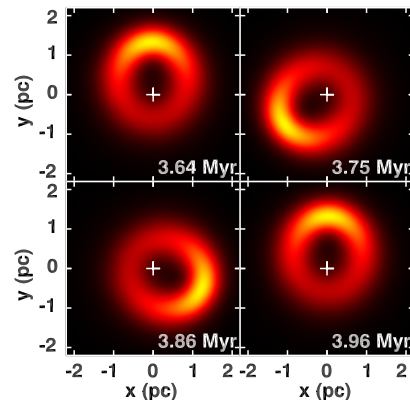


Figure 3. The projected density of the saturated configuration at the end of the simulation is followed over a precession cycle; a P1-like peak is evident around apse-alignment; the distribution is practically invariant as it revolves uniformly over its 0.32 Myr cycle.

sufficient eccentricity (through a CR instability) in the presence of a dominant eccentric perturber (the more massive eccentric and precessing prograde disk) Touma et al. (2009). One can presumably describe the inception of these cycles in a generalized Kozai-Lidov framework (Naoz et al. 2011), but then one is left with the harder task of accounting for the dispersal of the population on these cycles. We gained valuable insight into dispersal then saturation by modeling a closely related process in a 2D analog of the 3D cluster (Kazandjian & Touma, in preparation). The model in question permits a blow by blow account of the mutual sculpting of planar prograde and retrograde populations in terms of capture in, then escape from a drifting, trapping region in phase-space (Sridhar & Touma 1997). It can naturally explain the near-coplanar growth and apse alignment in phase **I** of 3D dynamics. Furthermore, it clarifies the collisionless damping process at work in the decaying cycles of phase **III**. How the eccentricity growth of phase **I** paves the way for inclination growth in phase **II** cannot be captured in a planar analogue and shall await a more sophisticated treatment of the 3D deployment of unstable CR clusters.

3 CONFRONTATION WITH M31: PRELIMINARY RESULTS

The saturated distribution of stars, which is followed in projection, and over a full precessional cycle in Fig. 3, generalizes Keplerian disk models of M31’s nucleus (Peiris & Tremaine 2003) in two obvious ways. On one hand, the eccentric disk in our nucleus is shrouded by a lighter triaxial cluster, whereas currently preferred models tend to work with the eccentric disk alone: as discussed below, the additional triaxial cluster contributes a crucial improvement to model kinematics. On the other hand, successful eccentric disk models (Peiris & Tremaine 2003) are essentially kinematic in nature (their origin, and dynamical evolution remaining uncertain), whereas ours is a dynamically stable nucleus to which an unstable configuration saturates. Given that the eccentric disk component in our saturated lopsided nucleus is ten times more massive than the triaxial cluster,

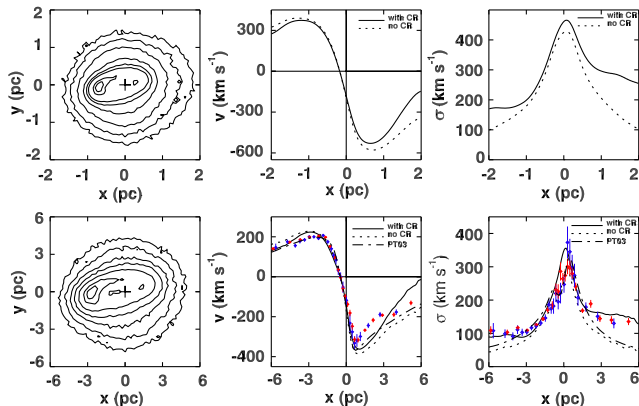


Figure 4. Photometry and kinematics of saturated configurations are probed, and a remarkable agreement with the kinematics of Andromeda’s nucleus is demonstrated. In the **top row**, we show the results of photometric and kinematic observations of our fiducial simulation: a double-peak is evident in the surface brightness distribution **[left]**, with a brighter (P1-like) peak on the left of the SMBH at the origin, and a fainter (P2-like) peak on its right; the zero point in the rotation curve **top [center]** is shifted towards brighter peak and slower rotation; the peak velocity dispersion is displaced towards fainter peak and faster rotation **[right]**; rotation and LOSVD curves are shown without (**dashed**) and with (**solid**) contributions from the dispersed CR disk, which contributions introduce a significant asymmetry in the tails. The best fit (non-aligned) models of Peiris & Tremaine (2003) (labeled PT03) with no bulge are also displayed as **dot-dashed** lines. A Quantitative agreement is demonstrated in the **bottom row, center and right panels**, between a dynamically similar copy of the featured simulation (observed under HST conditions) (**solid line**) and M31’s kinematics (Bender et al. 2005) (blue and red dots).

the photometry and kinematics of this nucleus will naturally display all the significant qualitative features which eccentric disk models seek to explain (Fig. 4, top row): a double peak in surface brightness, an asymmetry in the rotation velocity (with an off-center zero velocity point), and an off-centered peak in the line of sight velocity dispersion (Bender et al. 2005; Peiris & Tremaine 2003) (hereafter LOSVD). Pushing our luck, we seek a preliminary quantitative confrontation of simulation results with observations of M31’s nucleus. In so doing, we work with a rescaled and dynamically similar version of our fiducial experiment (roughly speaking, we rescale from fiducial simulation length scale $\simeq 1$ pc, to M31 nucleus scale, $\simeq 3$ pc). The resulting Model Nucleus is then observed under HST conditions (Bender et al. 2005; Peiris & Tremaine 2003) (details in Appendix A). The outcome of this procedure is then overlaid with M31’s kinematics (Fig. 4, bottom row). We closely match the observed shift in the zero-point of rotation curve ($x=-0.485$ compared to $x=-0.448$ pc in observations (Bender et al. 2005)), the difference in the peak rotation velocities ($v=585$ km s $^{-1}$ compared to $v=532 \pm 41$ km s $^{-1}$), the magnitude of and shift in the peak in the LOSVD curve ($x=+0.187$, $\sigma=+355.7$ km s $^{-1}$ compared to $x=0.298$ pc, $\sigma=+373 \pm 48$ km s $^{-1}$).

The triaxial cluster of our Model endows its kinematics with the marked asymmetry between the tails of the LOSVD, which is clearly observed in HST data (Kormendy & Bender 1999; Bender et al. 2005), and which

has proven difficult to recover with eccentric disks alone (Peiris & Tremaine 2003) (compare PT03 and the “no CR” curves to the solid curve in the rightmost column of Fig. 4). Recall that this cluster consists of eccentric orbits which result from the triaxial dispersal of the initially retrograde cluster (rows **b** and **d** of Fig. 1). When superposed over the more massive lopsided disk, stars in this cluster will leave their kinematic signature mostly in the outer parts of the nucleus, which is where they linger the most on their eccentric orbits. That signature is particularly pronounced where the lopsided prograde disk contributes least, i.e. on the anti-P1 side of the nucleus, hence the resulting asymmetry.

The initial ring-like configuration in our experiment is clearly deficient in stars in its central region. Hence, we did not expect for the resulting double nucleus to closely approximate the observed surface brightness profile in that region. This said, we were pleased to learn that a surface brightness profile, along a slit extending from brighter to fainter peak, has maxima around 13.3 and 14.2 mag.arcsec $^{-2}$ respectively, which compare favorably with the 13.2 and 13.57 mag.arcsec $^{-2}$, observed by HST.

Last but not least, we note that for the adopted similarity transformation¹ the pattern speed of the lopsided mode scales down from the 19 km s $^{-1}$ pc $^{-1}$ of the fiducial nucleus (Fig. 2, **d**), to the slower 4.3 km s $^{-1}$ pc $^{-1}$ of the Model Nucleus. At this relatively slow pattern speed, gravitational perturbations by the Model Nucleus are expected to drive and confine gas in a disk close to the SMBH (Chang et al. 2007). When fueled by stellar mass loss from the nucleus, such a disk can regenerate starbursts at a rate which is consistent with the observed compact cluster of early type stars (P3) around M31’s SMBH (Bender et al. 2005; Chang et al. 2007). Thus, M31’s P3 could very well be a direct consequence of P1 and P2 in our dynamical Model.

4 DISCUSSION

Andromeda’s kinematics shows a marked asymmetry between the tails of its LOSVD which is clearly unaccounted for in Keplerian disk models, and appears to be cleanly resolved by combining an eccentric disk with a triaxial cluster of highly eccentric orbits. To be sure, thorough modeling is called for before we can rigorously quantify the improvements of a disk-cluster combination over the thick eccentric disk model of Peiris & Tremaine (2003). Still, we find it remarkable that this combination achieves, with minimal probing, the level of qualitative and quantitative agreement described above, and to see it emerge as a natural end product of our process can only strengthen the case for CR stimuli of double nuclei (Lauer et al. 2005). That case is made stronger when one learns that a rich variety of CR configurations are equally prone to developing lopsidedness (details in Appendix B.). Experiments with CR point masses suggest that a cluster, initially on a circular trajectory, can drive a coplanar disk unstable provided its orbital radius is less than a critical radius (which is roughly equal to twice the

¹ In this transformation, time is rescaled by $s^{\frac{3}{2}}$, whenever length is rescaled by s . The adopted $s \simeq 2.7$ accounts for the slower precession rate of the Model Nucleus.

mean radius of the disk); clusters on highly inclined circular trajectories can still drive a CR disk into a lopsided state; on the other hand, clusters with too large an initial eccentricity will end up with little negative angular momentum to drive a coplanar disk lopsided. The CR perturbation envisaged in this work is delivered by a CR cluster which spirals deep into the nucleus by dynamical friction with bulge stars (Tremaine et al. 1975) before it disrupts in the combined tidal field of bulge and SMBH (Quillen & Hubbard 2003). The orbital radius at which the cluster disrupts depends critically on the cluster's core density. For a cluster migrating on a near-circular trajectory into M31's nucleus, we estimate (Quillen & Hubbard 2003) that a core density $\geq 5 \times 10^5 M_{\odot} \text{pc}^{-3}$ is sufficient for the cluster to cross past the critical radius for instability. Mass segregation and/or intermediate-mass black hole formation (Kim & Morris 2003; Fujii et al. 2010) can amplify core density significantly, thus further delaying disruption till the cluster migrates into the overlapping configurations explored here. Such configurations may also arise when a cluster penetrates the nucleus on an eccentric orbit, and disrupts upon close encounter with the SMBH. CR clusters will likely approach a pre-existing nuclear disk on eccentric, and inclined trajectories; they may thus find themselves on the eccentricity-inclination cycles observed above, then disperse as they drive the disk in a saturated lopsided configuration. Given on one hand the strong likelihood of counter-rotating excitations in galactic centers (Jog & Combes 2009), and on the other the robustness and efficiency of the proposed mechanism, double nuclei are likely to prove ubiquitous in stellar clusters dominated by super-massive black holes (Lauer et al. 2005). More generally (and irrespective of whether or not a given lopsided nucleus results from a CR instability), the proposed mechanism can be deployed to customize triaxial equilibrium configurations with which to model observed kinematics of stellar black hole nuclei (Alexander 2005) (the Milky Way's included) and improve estimates of the mass and feeding rate² of the black hole within (Magorrian et al. 1998; Kormendy 2004). Whether exploring realistic CR scenarios or tailoring triaxial equilibrium models, extensive numerical simulations of CR stellar systems with state of the art solvers (Fujii et al. 2010; Touma et al. 2009) will surely contribute invaluable insights into the dynamics and structure of stellar black hole nuclei.

ACKNOWLEDGMENTS

M.V.K. expresses his gratitude to the faculty, staff, and students of the department of physics at the American University of Beirut (AUB), where the bulk of this work was conducted. Computations were performed the Ibsina cluster at the Center of Advanced Mathematical Sciences(AUB), and on the Aurora cluster at the Institute of Advanced Studies (Princeton). Fruitful discussions with S. Sridhar,

Scott Tremaine and Jarle Brinchmann are gratefully acknowledged. The support of NSF grants AST-0206038 and AST-0507401 was invaluable during all phases of this work.

REFERENCES

- Alexander T., 2005, *Phys. Rep.*, 419, 65
 Bacon R., Emsellem E., Combes F., Copin Y., Monnet G., Martin P., 2001, *Astron. & Astrophys.*, 371, 409
 Bender R. et al., 2005, *Astrophys. J.*, 631, 280
 Chang P., Murray-Clay R., Chiang E., Quataert E., 2007, *Astrophys. J.*, 668, 236
 Dressler A., Richstone D. O., 1988, *Astrophys. J.*, 324, 701
 Emsellem E., Combes F., 1997, *Astron. & Astrophys.*, 323, 674
 Fujii M., Iwasawa M., Funato Y., Makino J., 2010, ArXiv e-prints
 Gerhard O., 2001, *Astrophys. J. Letters.*, 546, L39
 Gultekin K., Richstone D. O., Gebhardt K., Faber S. M., Lauer T. R., Bender R., Kormendy J., Pinkney J., 2011, ArXiv e-prints
 Hopkins P. F., Quataert E., 2010a, *Mon. Not. R. Astron. Soc.*, 407, 1529
 Hopkins P. F., Quataert E., 2010b, *Mon. Not. R. Astron. Soc.*, 405, L41
 Jacobs V., Sellwood J. A., 2001, *Astrophys. J. Letters.*, 555, L25
 Jog C. J., Combes F., 2009, *Phys. Rep.*, 471, 75
 Kim S. S., Morris M., 2003, *Astrophys. J.*, 597, 312
 Kormendy J., 1988, *Astrophys. J.*, 325, 128
 Kormendy J., 2004, *Coevolution of Black Holes and Galaxies*, 1
 Kormendy J., Bender R., 1999, *Astrophys. J.*, 522, 772
 Lauer T. R. et al., 2005, *Astron. J.*, 129, 2138
 Lauer T. R. et al., 1993, *Astron. J.*, 106, 1436
 Lauer T. R. et al., 1996, *Astrophys. J. Letters.*, 471, L79+
 Light E. S., Danielson R. E., Schwarzschild M., 1974, *Astrophys. J.*, 194, 257
 Magorrian J., Tremaine S., 1999, *Mon. Not. R. Astron. Soc.*, 309, 447
 Magorrian J. et al., 1998, *Astron. J.*, 115, 2285
 Naoz S., Farr W. M., Lithwick Y., Rasio F. A., Teyssandier J., 2011, ArXiv e-prints
 Peiris H. V., Tremaine S., 2003, *Astrophys. J.*, 599, 237
 Quillen A. C., Hubbard A., 2003, *Astrophys. J.*, 125, 2998
 Salow R. M., Statler T. S., 2001, *Astrophys. J. Letters.*, 551, L49
 Sambhus N., Sridhar S., 2002, *Astron. & Astrophys.*, 388, 766
 Silk J., 2011, ArXiv e-prints
 Springel V., 2005, *Mon. Not. R. Astron. Soc.*, 364, 1105
 Sridhar S., Saini T. D., 2010, *Mon. Not. R. Astron. Soc.*, 404, 527
 Sridhar S., Touma J., 1997, *Mon. Not. R. Astron. Soc.*, 292, 657
 Touma J. R., 2002, *Mon. Not. R. Astron. Soc.*, 333, 583
 Touma J. R., Tremaine S., Kazandjian M. V., 2009, *Mon. Not. R. Astron. Soc.*, 394, 1085
 Tremaine S., 1995, *Astron. J.*, 110, 628
 Tremaine S., 2001, *Astron. J.*, 121, 1776

² We note in passing that, as it drives a substantial fraction of stars to near radial orbits, the CR instability populates the loss cone of the SMBH (Magorrian & Tremaine 1999). Repeated CR accretion events will thus enhance the feeding rate of the central SMBH as they sculpt stellar distributions in its sphere of influence.

Tremaine S. D., Ostriker J. P., Spitzer, Jr. L., 1975, *Astrophys. J.*, 196, 407

A METHODS

We performed our simulations using the cosmological numerical tool *Gadget-2* (Springel 2005). Forces were evaluated using the oct-tree; cosmological, SPH, and grid capabilities were switched off. Although this narrowed down the parameter space significantly, one had to be careful fine tuning parameters which control tree walk and time stepping. The depth of the tree to be explored is controlled by *Gadget-2*'s parameter `ErrTolForceAcc`: daughter cells are opened until a certain criterion, set by `ErrTolForceAcc`, is satisfied, thus terminating the tree walk (we refer the reader to *Gadget-2*'s user guide for more details about this criterion). Once the accelerations of all the particles are at our disposal, the positions of these particles are advanced with a time-step $\Delta t = \sqrt{2\eta b/|\mathbf{a}|}$, where $|\mathbf{a}|$, η and ϵ are the magnitude of the computed acceleration, `ErrTolIntAccuracy` (which controls the step-size) and the gravitational softening respectively. Setting `ErrTolForceAcc` to 0.001 and `ErrTolIntAccuracy` to 0.001 assured accurate enough simulations for our purposes.

Our featured simulations consist of a massive prograde disk, on which a light retrograde disk is overlaid, with both residing in the sphere of influence of a central SMBH. Such a configuration is a likely outcome of the disruption of clusters that can migrate deep in the galactic centers (Gerhard 2001; Kim & Morris 2003; Fujii et al. 2010). Initial positions and velocities of disk particles are picked from radial and vertical distributions which are standard to disk dynamics simulations (Emsellem & Combes 1997). Since *Gadget-2* has difficulties in dealing with high mass density contrast, we further chose our disk to be annular in-order to avoid close encounters with the SMBH. Thus, we introduced an inner and outer radial cut-off when sampling the disks. The SMBH is modeled as a Plummer-softened particle with softening length of $b=0.01$ pc. To minimize sources of instability which are not related to counter-rotation, disk components were separately virialized before coupling them to each other or to perturbers. In the course of virializing, the more massive disks (prograde in our simulations) underwent short-lived gravitational instabilities, before relaxing to a hotter near-axisymmetric equilibrium state.

The central SMBH with a mass of $10^8 M_\odot$ is ten times more massive than the pre-existing disk of stars, itself ten times more massive than the disturbing CR disk. The mean eccentricities of the virialized prograde and retrograde disk were $\langle e_p \rangle = 0.22$ and $\langle e_r \rangle = 0.25$ respectively, with corresponding standard deviations $\sigma_p = 0.12$ and $\sigma_r = 0.14$. In both disks, the mean of the semi-major axis distribution was $\langle a \rangle \sim 1.06$ pc with a standard deviation of ~ 0.3 pc whereas the spread in inclination was around 8° .

Simulation particles revolve around the central SMBH on perturbed Keplerian ellipses; associated osculating orbital elements [namely semi-major axis (a), eccentricity (e), inclination (I), argument of periapse (g), and longitude of the node (h)] are simply recovered from particle position and velocity. In addition to particle orbit elements, our dynamical analysis required the time evolving Fourier modes

of the surface (projected) density of the CR cluster, and associated potentials. The surface density $\Sigma(r, \theta, t)$ is Fourier expanded in θ :

$$\Sigma(r, \theta, t) = a_0(r, t) + \sum_{m=1}^{m=\infty} a_m(r, t) \cos(m\theta + \phi_m(r, t)) \quad (\text{A-1})$$

with $[a_m(r, t), \phi_m(r, t)]$, the m^{th} mode amplitude and phase respectively. This is practically performed with FFTs over a grid in θ at various judiciously chosen radii. The relative power K_m in a given mode m is then computed

$$K_m(t) \equiv \frac{\int_0^\infty a_m^2(r, t) 2\pi r dr}{\sum_{m=0}^\infty \int_0^\infty a_m^2(r, t) 2\pi r dr}, \quad (\text{A-2})$$

Cluster kinematics were determined from a snapshot of our benchmark 3D simulation at $T=4$ Myr (well into the saturated regime). The scale length of that simulation is on the order of 1 pc, whereas that of M31's nucleus is more like 3 pc. To compare with M31 observations, we rescaled positions (and with them the softening length) by a factor s , and time by a factor $s^{3/2}$; velocities are naturally rescaled by $s^{-1/2}$ to leave equations of motion in the new variables invariant. The adopted scaling ($s \simeq 2.7$) was first constrained within the interval $2.0 < s < 3.1$, by matching peaks in the rotation curve, then fine tuned to fit the kinematics, while adjusting the sky angles as well.

While searching for the optimal sky angles (Peiris & Tremaine 2003) of our rescaled snapshot, we took into account artifacts of the HST SITS instrument by convolving all the particles with a double Gaussian (Bender et al. 2005). The slit width was set to $0.1''$ with a PA of 39° . Both the fiducial, and rescaled snapshots were observed with the same sky angles $\theta_a = -59.1^\circ$, $\theta_i = 65.3^\circ$. We note that larger θ_i permits an almost perfect match with the observed LOSVD (remarkably so for θ_i close to M31's inclination of 77°), with deteriorating rotation curve; while smaller θ_i improved the fit to the rotation curve dramatically while disturbing agreement in the LOSVD.

B THE CR INSTABILITY EXPLORED

Here, we summarize results of a battery of experiments conducted with CR configurations that are likely to occur in galactic centers.

First, we explore dynamics in highly inclined configurations, by considering an extreme situation: a lower resolution (50×10^3 particles) analogue of the 3D benchmark simulation was evolved with equal mass annuli ($M_r = M_p = 0.05 M_\bullet$, M_r and M_p are the masses of the retrograde and prograde disks respectively) where the PP and RP disks have a relative inclination of 90° . This experiment was motivated by our concern about non-coplanar, CR rings in galactic centers, and whether such configuration may result in $m=1$ instabilities. The configuration which was violently unstable, resulted in both components merging, then relaxing into a thick, precessing, and lopsided disk.

Second, we explored the effect of an in-spiraling cluster on our annular disk (Fujii et al. 2010). Evolving an actual realization of a plummer sphere with *Gadget-2* around the

SMBH with enough accuracy is prohibitively expensive, thus the cluster was modeled as a point mass with a large softening radius 0.1 pc. The point mass was put on a retrograde Keplerian orbit around the SMBH. The massive disk of our 3D simulation was used as the prograde component ($M_p=0.1 M_\bullet$, $\langle a \rangle=0.92$ pc), but with 25×10^3 particles instead of 250×10^3 . The default values of the point mass (cluster) orbit are $M_c=0.01 M_\bullet$ (M_c is the mass of the cluster), semi-major axis $a_c=0.9$ pc, eccentricity $e_c=0$, and inclination $I_c=180^\circ$. The simulations for this scenario consisted of four suites. In each suite one parameter was varied while keeping the remaining parameters to their default value:

- **Suite 1.** M_c was varied from 0.001 to $0.1 M_\bullet$: The prograde disk developed an $m=1$ mode for $M_c > 0.01 M_\bullet$.
- **Suite 2.** The inclination of cluster was varied from 90° to 180° : In all cases the cluster and the disk ended up in the same plane, and with an $m=1$ growing instability mode when the relative inclination was larger than 90° .
- **Suite 3.** The eccentricity was varied from 0 to 0.9: the low eccentricity $m=1$ growing instability shuts off for $e_c > 0.6$.
- **Suite 4.** The semi-major axis was varied from 0.8 to 10 pc: for $a_c > 2\langle a \rangle$ the annulus remained axisymmetric, with an $m=1$ modes growing for $a_c < 2\langle a \rangle$